Nanoscale

PAPER

View Article Online
View Journal | View Issue

Cite this: *Nanoscale*, 2015, **7**, 4048

NaF-mediated controlled-synthesis of multicolor Na_xScF_{3+x}:Yb/Er upconversion nanocrystals†

Wen-Bo Pei,[a] Bo Chen,[a] Lili Wang,[a] Jiansheng Wu,[b] Xue Teng,[a] Raymond Lau,*[a] Ling Huang*[c] and Wei Huang[c]

Received 10th November 2014,
Accepted 26th January 2015

DOI: 10.1039/c4nr06637e

www.rsc.org/nanoscale

Synthesis of lanthanide-doped upconversion nanocrystals (LDUNs) with controlled morphology and luminescence has long been desired in order to fulfill various application requirements. In this work, we have investigated the effect of the NaF : Ln^{3+} molar ratio, in the range of 1 to 20, on the morphology, crystal structure, and upconversion properties of Na_xScF_{3+x}:Yb/Er nanocrystals that are reported to possess different upconversion properties from those of $NaYF_4$:Yb/Er nanocrystals. The experimental results prove that the NaF : Ln^{3+} molar ratio influences significantly the growth process of the nanocrystals, *i.e.* a low NaF : Ln^{3+} molar ratio results in hexagonal $NaScF_4$ nanocrystals, while a high NaF : Ln^{3+} molar ratio favors monoclinic Na_3ScF_6 nanocrystals. When the NaF : Ln^{3+} molar ratio is as high as 6 or above, phase separation is found and hexagonal $NaYbF_4$ nanocrystals showed up for the first time. Simply by adjusting the NaF : Ln^{3+} molar ratio, we have successfully achieved the simultaneous control of the shape, size, as well as the crystallographic phase of the Na_xScF_{3+x}:Yb/Er nanocrystals, which give different red to green (R/G) ratios (integral area), leading to a multicolor upconversion luminescence from orange-red to green. This study provides a vivid example to track and interpret the formation mechanisms and growth processes of Na_xScF_{3+x}:Yb/Er nanocrystals, which shall be instructive for guiding the controlled synthesis of other LDUNs and extending their according applications in optical communication, color display, anti-counterfeiting, bioimaging, and so on.

1 Introduction

Photon upconversion (UC) has attracted increasing research interest for decades since its first recognition and formulation by Auzel and Ovsyankin in the mid-1960s,[1–5] whereas lanthanide ion (Ln^{3+}) doped luminescent materials have shown an excellent near infrared (NIR) to visible UC efficiency, with unparalleled advantages, including but not limited to narrow emission bands, long luminescence lifetimes (micro- to millisecond range), low cytotoxicity, and high resistance to photobleaching, photoblinking and photochemical degradation.[6,7] These unique characteristics have offered them wide applications in areas ranging from high-resolution displays, integrated optical systems, substitutes for organic dyes, solid-state lasers, to biological labels, optical communication, and so on.[8–18]

Among all the lanthanide-based host materials observed to date including oxides, phosphates, and vanadates,[19–23] fluorides are proved to be the most efficient hosts for visible UC luminescence, due to their intrinsically low phonon energies, which lead to a decrease in the nonradiative relaxation rate that affects the UC efficiency.[24–33] $NaMF_4$:Yb/Ln (M = Y, La, Gd or Lu, Ln = Er or Tm) UC nanocrystals showing various crystal structures, morphology as well as UC luminescence have been systematically investigated in the last 10 years.[9,34–38] The effects of the experimental factors such as the reaction time and temperature, the chemical composition and the polarity of the solvents, the F^- : Ln^{3+} molar ratio, as well as the synthesis procedure on the structure and dimensions of the $NaMF_4$:Yb/Ln nanocrystals have been studied extensively.[39–41]

However, except few recent reports on the synthesis and UC luminescence of Na_xScF_{3+x} nanocrystals, there is a lack of a systematic study on the controlled synthesis of Na_xScF_{3+x} nano-

[a]*School of Chemical and Biomedical Engineering, Nanyang Technological University, 62 Nanyang Drive, 637459, Singapore. E-mail: WMLau@ntu.edu.sg*
[b]*School of Materials Science and Engineering, Nanyang Technological University, 50 Nanyang Ave, 639672, Singapore*
[c]*Key Laboratory of Flexible Electronics (KLOFE) & Institute of Advanced Materials (IAM), Jiangsu National Synergistic Innovation Center for Advanced Materials (SICAM), Nanjing Tech University (NanjingTech), 30 South Puzhu Road, Nanjing, 211816, P.R. China. E-mail: iamlhuang@njtech.edu.cn*

†Electronic supplementary information (ESI) available: HRTEM images and EDS data of the $NaScF_4$:Yb/Er and Na_3ScF_6:Yb/Er nanocrystals. TEM images of Na_xScF_{3+x}:Yb/Er nanocrystals synthesized at NaF:Ln^{3+} molar ratios of 14 and 20. XRD patterns of the Na_xScF_{3+x}:Yb/Er nanocrystals synthesized at NaF:Ln^{3+} molar ratios of 6, 8, 10, 14 and 20. XRD patterns of the $NaYF_4$:Yb/Er and $NaGdF_4$:Yb/Er nanocrystals synthesized at a NaF:Ln^{3+} molar ratio of 10. XRD and UC luminescence spectra of the corresponding $NaYF_4$:Yb/Er, $NaYbF_4$:Er and ultra-small Na_3ScF_6:Yb/Er nanocrystals. See DOI: 10.1039/c4nr06637e

crystals under varying experimental conditions.[42,43] What is more, since Sc^{3+} possesses the smallest rare earth ionic radius and distinct atomic electronic configuration, Sc^{3+} ion-based UC nanocrystals usually give a strong red UC luminescence at 660 nm,[44] which is different from those of $NaMF_4$:Yb/Er (M = Y, La, Gd or Lu) nanocrystals. Thus, it is even worth carrying out a systematic exploration of the effect of varying experimental conditions on the obtained Na_xScF_{3+x} nanocrystals and further on their UC luminescence.

Suitable applications normally require the UC nanocrystals to have precise parameters, such as size, shape, crystallographic phase, chemical composition, and the desired luminescence properties. In addition, the nanocrystals should be uniformly shaped while maintaining a high-monodispersion and well-defined crystalline structure. Hence, controllable synthesis of the nanocrystals with the desired parameters and UC luminescence has long been remained a challenging topic,[45–47] and a comprehensive understanding of the process of nanocrystal growth and the cause of phase transition will provide straightforward clues to solve such challenges.

In this paper, a controlled synthesis of Na_xScF_{3+x}:Yb/Er nanocrystals at different shapes, sizes, and crystallographic phases is achieved simply by adjustment of the $NaF:Ln^{3+}$ molar ratio. In addition, phase separation and hexagonal $NaYbF_4$ nanocrystals are observed at a higher $NaF:Ln^{3+}$ molar ratio for the first time. The according UC luminescence of each product and the possible energy transfer mechanism are also discussed.

2 Experimental section

2.1 Chemicals and materials

All the starting chemicals and reagents used in the experiments, including $ScCl_3{\cdot}6H_2O$ (99.99%), $YbCl_3{\cdot}6H_2O$ (99.9%), $ErCl_3{\cdot}6H_2O$ (99.9%), NaF(99%), 1-octadecene (90%), oleic acid (90%), alcohol (95%), and cyclohexane (99.9%) were purchased from Sigma-Aldrich and used as received.

2.2 Nanocrystal synthesis

1 mmol $RECl_3{\cdot}6H_2O$ (0.78 mmol $ScCl_3{\cdot}6H_2O$, 0.2 mmol $YbCl_3{\cdot}6H_2O$, 0.02 mmol $ErCl_3{\cdot}6H_2O$) was added to a 50 mL flask containing 12.5 mL oleic acid and 12.5 mL 1-octadecene. The solution was heated to 160 °C under argon protection. Subsequently, an appropriate amount of NaF (1, 1.5, 2, 2.5, 4, 5, 6, 8, 10, 14 and 20 mmol) according to the desired product phase and chemical composition, was added directly to the solution. After 30 minutes of stirring, the solution was heated to 300 °C directly under an argon environment for 1.5 h with vigorous magnetic stirring. Ethanol was added to the solution after cooling down to room temperature, and the resulting nanocrystals were collected by centrifugation, washed with the mixture of water and ethanol several times, and finally re-dispersed in cyclohexane.

2.3 Characterization

The morphology and structure of the nanocrystals were characterized by using a low resolution (JEOL JEM-1400) transmission electron microscope (TEM) operated at an accelerating voltage of 100 kV and high resolution TEM (HRTEM) (JEOL JEM-3010) operated at an accelerating voltage of 300 kV. Energy Dispersive X-ray Spectrometry (EDS) measurement was collected using the JED-2300 Analysis Station operated at 20 kV. The crystallographic information of the samples was obtained by the X-ray diffraction (XRD) measurements, using a Bruker D2 Phaser XRD with Cu Kα radiation (λ = 1.5406 Å) from 10° to 70° at a step of 0.1° s^{-1}. The UC luminescence spectra were recorded on a Horiba Jobin Yvon FluoroMax-4 system and an external MDL/MDL-H-980 nm CW laser system was used as the excitation source. The nanocrystals were dispersed in cyclohexane (1 wt%) in a standard quartz cuvette at room temperature to measure the UC luminescence spectra.

3 Results and discussion

TEM images of the Na_xScF_{3+x}:Yb/Er nanocrystals synthesized at $NaF:Ln^{3+}$ molar ratios of 1 (a), 1.5 (b), 2 (c), 2.5 (d), 4 (e) and 5 (f) are shown in Fig. 1. It can be seen that the shape of the nanocrystals synthesized at different $NaF:Ln^{3+}$ ratios changes from nanospheres at the low $NaF:Ln^{3+}$ ratio, *i.e.*, 1, to the mixture of both nanospheres and nanocubes at the $NaF:Ln^{3+}$ ratio of 1.5, then big nanorods, nanospheres, nanocubes and eventually small nanopolyhedra at higher $NaF:Ln^{3+}$ molar ratios of 2, 2.5, 4 and 5 respectively. Moreover, the size of the obtained nanocrystals increases gradually from 18.2 nm to 57.6 nm as the $NaF:Ln^{3+}$ molar ratio increases from 1 (a) to 4 (e), and then sharply decreases at the $NaF:Ln^{3+}$ ratio of 5 (f). The results clearly demonstrate that the $NaF:Ln^{3+}$ molar ratio, which is responsible for the shape and size evolution, has a great impact on the dynamic process governing nucleation and growth of the Na_xScF_{3+x} nanocrystals.

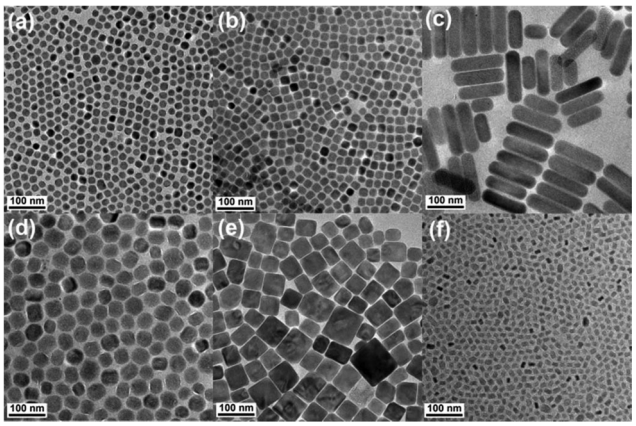

Fig. 1 TEM images of Na_xScF_{3+x}:Yb/Er nanocrystals synthesized at $NaF:Ln^{3+}$ molar ratios of 1 (a), 1.5 (b), 2 (c), 2.5 (d), 4 (e) and 5 (f), respectively.

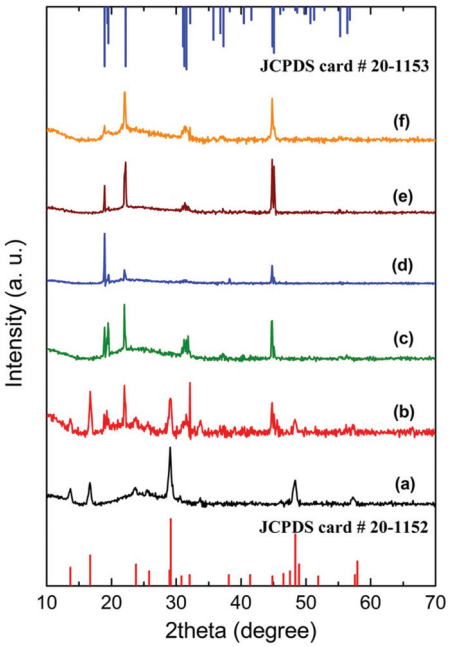

Fig. 2 XRD patterns for the nanocrystals synthesized at $NaF : Ln^{3+}$ molar ratios of 1 (a), 1.5 (b), 2 (c), 2.5 (d), 4 (e) and 5 (f) respectively (blue and red lines at the top and bottom are the standard XRD patterns of the monoclinic phase Na_3ScF_6 nanocrystals (JCPDS card no. 20-1153) and the hexagonal phase $NaScF_4$ nanocrystals (JCPDS card no. 20-1152)).

XRD patterns were collected and shown in Fig. 2 to confirm the crystallographic phases of the nanocrystals synthesized under each individual experimental conditions. It can be found that pure hexagonal phase $NaScF_4$ (JCPDS 20-1152) nanocrystals can only be observed at the $NaF : Ln^{3+}$ molar ratio of 1 (a), while pure monoclinic phase Na_3ScF_6 (JCPDS 20-1153) nanocrystals can be collected at a wide $NaF : Ln^{3+}$ molar ratio range condition from 2 to 5 (c, d, e, f). A moderate $NaF : Ln^{3+}$ molar ratio of 1.5 results in a mixture of both hexagonal and monoclinic phases (b). HRTEM images of the resulting $NaScF_4$:Yb/Er and Na_3ScF_6:Yb/Er nanocrystals are shown in Fig. S1.† Lattice fringes of $NaScF_4$:Yb/Er and Na_3ScF_6:Yb/Er nanocrystals were observed to have a *d*-spacing of 0.307 nm and 0.402 nm respectively, corresponding to the distance of the (221) planes of $NaScF_4$ and (110) planes of the Na_3ScF_6 phase. Lattice parameters for both hexagonal and monoclinic Na_xScF_{3+x}:Yb/Er phases were calculated based on the XRD patterns. The results show the cell parameters of a = 13.0548 Å, c = 9.2099 Å and V = 1359.33 Å^3 for hexagonal as well as a = 5.6053 Å, b = 5.8520 Å, c = 8.0867 Å, and V = 265.25 Å^3 for the monoclinic phase. Both cell volumes are slightly higher than those of the standard data (V = 1350.49 Å^3 and 264.17 Å^3 respectively), which indicates the formation of Yb/Er doped Na_xScF_{3+x} nanocrystals because the Yb^{3+} and Er^{3+} ions of the larger ionic radii partially substitute the Sc^{3+} ions of smaller ionic radii. Composition analysis of the as-prepared Na_xScF_{3+x}:Yb/Er nanocrystals by using EDS reveals that the nanocrystals are mainly composed of Na, Sc, Yb, F and a small amount of Er element. It confirms the successful doping of Yb^{3+} and Er^{3+} ions in the host lattice in a direct manner (Fig. S2†).

The crystallographic phases agree well with the morphology evolution observed in Fig. 1. As is known that nanocrystals with a hexagonal phase usually give hexagonal plates or hexagonal prisms in an external format, while a monoclinic phase shows rod or block shaped mostly. Sphere-like to some extent, is a characteristic feature of small polyhedra under the TEM measurement. Obviously, the crystallographic phase evolution from hexagonal phases to mixed phases, and then the monoclinic phase gives a reasonable explanation for the shape development of the Na_xScF_{3+x}:Yb/Er nanocrystals. It is also noticed that the intensity of the relative diffraction peaks for the monoclinic phase in the XRD patterns switches with the morphologies evolution, suggesting the existence of preferential orientation as well as the versatile morphologies.

The above results indicate clearly that, at a low $NaF : Ln^{3+}$ molar ratio of 1, the hexagonal phase $NaScF_4$ is formed, while at a high $NaF : Ln^{3+}$ molar ratio (2–5), the monoclinic phase Na_3ScF_6 is favored. It is reported that the growth of the as-prepared Na_xScF_{3+x}:Yb/Er nanocrystal started with the reaction between F^- ions and rare earth oleate complexes.[48] A high F^- content can significantly accelerate the particle nucleation rate. A much faster nucleation speed results in a thermodynamically determined reaction process.[45] The corresponding thermodynamically stable phase monoclinic Na_3ScF_6 nanocrystals are formed. The size and morphology of the resulting nanocrystals are dependent on the dynamic process. The capping effect of F^- on the crystal surface would alter the average number of dangling bonds, and further change the chemical potential of the crystal, as well as the crystal plane.[45] Different NaF contents involved in each reaction conditions will cause the relative growth rate on different directions changing accordingly, leading to different crystal morphologies and sizes. In contrast, at a low $NaF : Ln^{3+}$ molar ratio, which means a low F^- content, nucleation and nanocrystal growing becomes quite slow and metastable hexagonal phase $NaScF_4$ nanocrystals are formed.

Na_xScF_{3+x}:Yb/Er nanocrystals prepared at much higher $NaF : Ln^{3+}$ molar ratios, *i.e.*, 6, 8, 10, 14 and 20 were also investigated and the corresponding TEM images are shown in Fig. 3 and S3.† Different from the previous ones which show quite uniform morphologies, a mixture of both small nanoparticles and big hexagonal plates was found. As the $NaF : Ln^{3+}$ molar ratio increases from 6 to 8, and further to 10, besides a small quantity of big hexagonal plates with a mean size of 150 nm in diameter and 80 nm in thickness is observed within the samples (Fig. 3d), and the rest of the majority of small nanocrystals decreases from 18.0 nm (Fig. 3a) to 10.5 nm (Fig. 3b), and finally to 8.2 nm (Fig. 3c). Along with the $NaF : Ln^{3+}$ molar ratio further increasing, *i.e.*, 14 and 20, the tiny nanocrystals reach a minimum diameter at about 8.0 nm (Fig. S3†) and remain constant. Nanocrystals with such obviously different morphologies observed in one sample are never reported in Na_xScF_{3+x}:Yb/Er nanocrystals, which may indicate the mixture of dramatically different crystal phases. XRD patterns shown

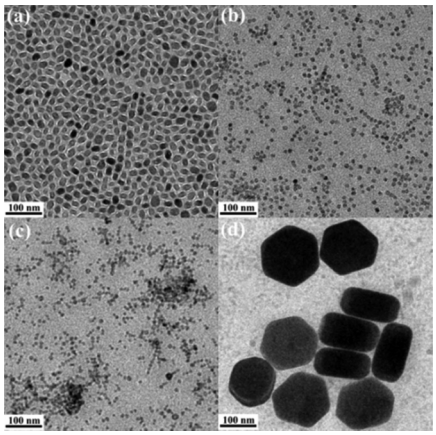

Fig. 3 TEM images of Na_xScF_{3+x}:Yb/Er nanocrystals synthesized at NaF : Ln^{3+} molar ratios of 6 (a), 8 (b), 10 (c) and the corresponding $NaYbF_4$ hexagonal plates (d), respectively.

in Fig. S4† prove the mixture of both monoclinic phase Na_3ScF_6 and hexagonal phase $NaYbF_4$ nanocrystals. Obviously, the majority of small nanoparticles belong to the Na_3ScF_6 nanocrystals, while the big hexagonal plates are the $NaYbF_4$ nanocrystals. The broadening peak width for Na_3ScF_6 nanocrystals as well as the narrow peak width for the $NaYbF_4$ crystal phase observed from the XRD patterns gives an indirect evidence illustrating the conclusion. Such a particular phase separation phenomenon has never been reported before. Comparison experiments for $NaMF_4$:Yb/Er (M = Y and Gd) nanocrystals synthesized at a NaF : Ln^{3+} molar ratio of 10 were done under the same process. XRD patterns shown in Fig. S5† demonstrate clearly that no phase separation phenomenon can be observed in the Y^{3+}/Gd^{3+} ion-based UC systems. Thus, phase separation is a particular phenomenon in the Sc^{3+} ion-based UC system. Considering that there is a big difference of rare earth ionic radius of Sc and doping ions, phase separation may occur under the condition when there is a quite fast nucleation rate at a much higher NaF content. Furthermore, crystallographic phase difference between Na_xScF_{3+x} and Na_xYbF_y systems should be another important reason. The monoclinic phase Na_3ScF_6 is formed at a high NaF : Ln^{3+} molar ratio. However, there is no monoclinic phase found for the Na_xYbF_y system. Phase separation under the high NaF:Ln^{3+} molar ratio condition is realized.

The findings clearly show that the NaF content can influence the growth process significantly and allow simultaneous control of the shape, size, as well as the crystallographic phase of the Na_xScF_{3+x}:Yb/Er nanocrystals. In other words, a simple tuning of the NaF content can be used to synthesize Na_xScF_{3+x}:Yb/Er nanocrystals with a controllable morphology and a crystallographic phase. Furthermore, phase separation is found and investigated for the first time in the Na_xScF_{3+x}:Yb/Er nanocrystals system.

To investigate the effect of the nanocrystal morphology and phase on the UC emission of the Na_xScF_{3+x}:Yb/Er nanocrystals, luminescence spectra were collected under 980 nm laser excitation. In the UC spectra shown in Fig. 4, three characteristic peaks located at 408, 541, and 654 nm can be found in all the samples. The emission band centered at 408 nm can be ascribed to the $^2H_{9/2} \rightarrow {}^4I_{15/2}$ transition of Er^{3+} ions. Green UC emissions at 510–560 nm and red UC emission at 640–670 nm can be ascribed to $^2H_{11/2} \rightarrow {}^4I_{15/2}$ and $^4S_{3/2} \rightarrow {}^4I_{15/2}$ transitions and Er^{3+} $^4F_{9/2} \rightarrow {}^4I_{15/2}$ transition of Er^{3+}, respectively.[49,50] Fig. 5

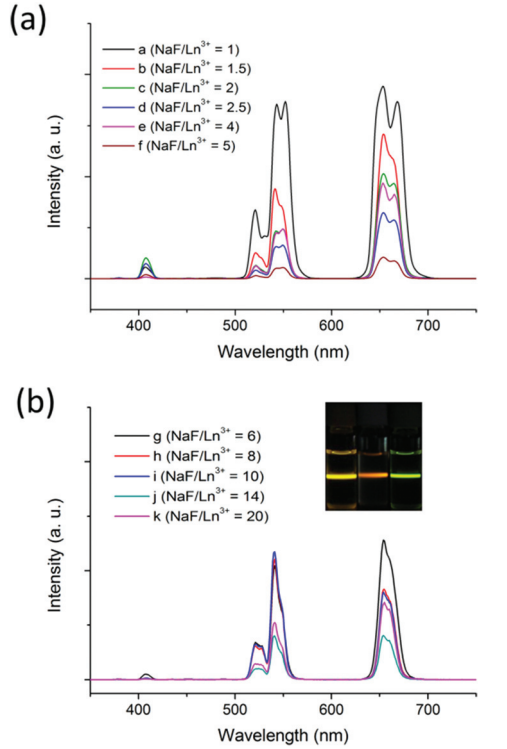

Fig. 4 UC luminescence spectra of the corresponding Na_xScF_{3+x}:Yb/Er nanocrystals synthesized at different NaF : Ln^{3+} molar ratios. The inset shows the corresponding PL photographs of nanoparticles synthesized at NaF : Ln^{3+} molar ratios of 1 (left), 2 (middle) and 10 (right) dispersed in cyclohexane.

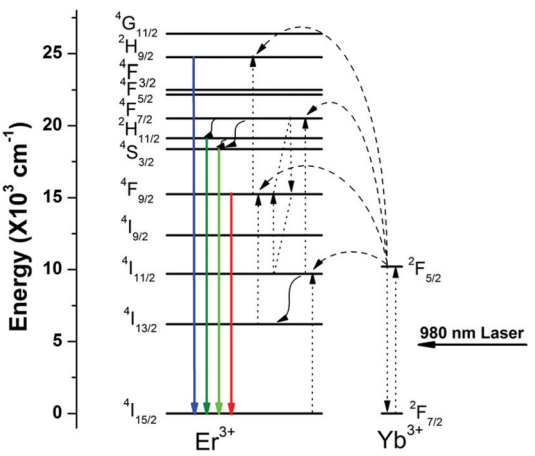

Fig. 5 UC energy transfer mechanism of the Na_xScF_{3+x}:Yb/Er nanocrystals.

Table 1 Effect of NaF content on the shape, size, crystallographic phase, and the R/G ratio of the Na_xScF_{3+x}:Yb/Er nanocrystals

NaF : Ln^{3+}	Shape	Size (Na_xScF_{3+x}) nm^{-1}	Crystallographic phase	R/G ratio
1	Nanosphere	18.2 ± 1.0	Hexagonal phase (H)	1.2852
1.5	Nanosphere & Nanocube	23.0 ± 0.8	Mixture of H and M	1.8333
2	Nanorod	(138.5 ± 2.5) × (39.4 ± 1.2)	Monoclinic phase (M)	2.4379
2.5	Nanosphere	43.5 ± 1.6	M	2.2500
4	Nanocube	57.6 ± 5.7	M	2.2055
5	Nanopolyhedron	17.8 ± 1.1	M	2.1657
6	Nanopolyhedron & Hexagonal plate	18.0 ± 0.7	Mixture of M and $NaYbF_4$	1.3681
8	Tiny particle & hexagonal plate	10.5 ± 0.3	Mixture of M and $NaYbF_4$	0.8184
10	Tiny particle & hexagonal plate	8.2 ± 0.4	Mixture of M and $NaYbF_4$	0.7337
14	Tiny particle & hexagonal plate	8.0 ± 0.3	Mixture of M and $NaYbF_4$	1.0743
20	Tiny particle & hexagonal plate	8.0 ± 0.3	Mixture of M and $NaYbF_4$	1.4063

shows the details of the UC energy transfer mechanism of Na_xScF_{3+x}:Yb/Er nanocrystals.

It is noticed that all the Na_xScF_{3+x}:Yb/Er nanocrystals show higher R/G ratios than those of $NaYF_4$:Yb/Er nanocrystals. It is found that the latter ones generally give strong green emission with a small R/G ratio (Table 1 and S6†), while Sc^{3+} ion-based nanocrystals show distinctive UC emission with enhanced red UC emission due to the small radius of the Sc^{3+} ion.[44] The small radius of the Sc^{3+} ion results in a shorter Sc^{3+}–Sc^{3+} distance compared to that of Y^{3+}–Y^{3+} with similar fluoride bridged moieties inside the host crystal. A short Sc^{3+}–Sc^{3+} distance leads to a short doping ions distance of Yb^{3+}–Er^{3+} cation-pairs. On the other hand, a Ln^{3+} (Yb^{3+} and Er^{3+} ions) cluster may exist because of the strong structural inhomogeneity due to the large cationic radius difference between Sc^{3+} and Ln^{3+}. The short distance between Ln^{3+} ions within Na_xScF_{3+x} host nanocrystals could enhance the cross relaxation ($^4F_{7/2}$ + $^4I_{11/2}$→$^4F_{9/2}$ + $^4F_{9/2}$). It diminishes the population in $^2H_{11/2}$ and $^4S_{3/2}$ levels and enhances the population in the $^4F_{9/2}$ energy level of Er^{3+}. Consequently, the Na_xScF_{3+x}:Yb/Er nanocrystals show enhanced red emission centered at 660 nm and the R/G ratio becomes higher than that of $NaYF_4$ host nanophosphors.

Moreover, it is worth noting that multicolor UC luminescence can be successfully realized in the Na_xScF_{3+x}:Yb/Er nanocrystals (inset of Fig. 4). Hexagonal phase $NaScF_4$:Yb/Er nanocrystals give bright yellow UC luminescence with the R/G ratio of 1.2852 and the overall UC intensity is obviously stronger than that of monoclinic Na_3ScF_6:Yb/Er ones. The monoclinic phase Na_3ScF_6:Yb/Er nanocrystals show orange-red color UC luminescence with a R/G ratio >2.16, while the mixed phases of both Na_3ScF_6 and $NaYbF_4$ show green color UC luminescence with a small R/G ratio, *i.e.* 0.7337. The results agree well with what have been reported before.[43,44,51] As there exists multiple independent sites for both Yb^{3+} and Er^{3+} in the hexagonal phase $NaScF_4$, which could increase the number of possible Yb^{3+} to Er^{3+} energy transfer processes, especially for the $^2H_{11/2} \rightarrow {}^4I_{15/2}$ and $^4S_{3/2} \rightarrow {}^4I_{15/2}$ transition processes. Thus a much stronger bright yellow color UC luminescence is achieved. For the monoclinic Na_3ScF_6:Yb/Er nanostructures, the R/G ratios are similar for the four samples and all show similar orange-red color UC luminescence. However, the overall UC intensity is different. The nanorods and nanocubes give the strongest UC luminescence, then the nanospheres and finally the nanopolyhedra. The results are reasonable as nanocrystals with good crystallinity and larger size, implying fewer surface defects and more luminescent centers deeply inside, could enable the luminescence processes more effectively. As for the green color UC luminescence found within the mixed phases of both Na_3ScF_6 and $NaYbF_4$, it is believed that the green color emission mainly arose from the Na_3ScF_6 nanocrystals with a low doping level of Yb and Er ions. A comparison experiment for $NaYbF_4$:Er nanocrystals was performed initially and it showed yellow color UC luminescence (Fig. S7†). However, it is reported that low doping levels of Yb and Er ions, *i.e.*, 1 mol% Er^{3+}/2 mol% Yb^{3+} codoped Na_3ScF_6 microcrystals show strong green UC luminescence.[52] Moreover, separate phases of the ultra-small Na_3ScF_6:Yb/Er and large $NaYbF_4$:Er nanocrystals for the sample at a NaF/Ln^{3+} molar ratio of 10 were collected for UC luminescence comparison and the results are shown in Fig. S8.† It can be seen that the ultra-small Na_3ScF_6:Yb/Er nanocrystals showed stronger emission with an R/G ratio of 0.7064 and gave green color emission; while the large $NaYbF_4$:Er nanocrystals showed weaker emission with an R/G ratio of 0.9564 and gave yellow color emission. As the amount of $NaYbF_4$ is quite low, mixed phases of a large amount of Na_3ScF_6:Yb/Er and a small amount of $NaYbF_4$:Er nanocrystals showed an overall green color emission with an R/G ratio of 0.7337 and the green color emission mainly arose from the UC luminescence contribution of the Na_3ScF_6:Yb/Er nanocrystals. As the NaF : Ln^{3+} molar ratio was further increased beyond 10, much more $NaYbF_4$:Er were formed gradually and the R/G ratio was increased. When the NaF : Ln^{3+} molar ratio reached 20, nearly no Yb and Er ions were embedded into the Na_3ScF_6 host lattice; yellow color UC luminescence originated from the $NaYbF_4$:Er nanocrystals.

4 Conclusions

Na_xScF_{3+x}:Yb/Er nanocrystals with controllable shape (nanospheres, nanorods, nanocubes and nanopolyhedra), size (from hundreds of nanometers to sub-ten nm), and crystallographic phase (monoclinic, hexagonal and their mixture) are

synthesized simply by the adjustment of the $NaF:Ln^{3+}$ molar ratio in the range of 1 to 20. Phase separation is observed for the first time at a high $NaF:Ln^{3+}$ molar ratio range (>6). The Na_xScF_{3+x}:Yb/Er nanocrystals show a higher R/G ratio than those of $NaYF_4$:Yb/Er. More importantly, multicolor emissions from orange-red, yellow to green can be achieved, which demonstrates that this series of host materials, Na_xScF_{3+x}, has promising applications in optical communication, high resolution three-dimensional bioimaging, color displays, solid-state lasers, photocatalysis, and photodynamic therapy.

Acknowledgements

R. L. thanks the financial support from NEA ETRP Grant (ref no.: 1102 108). L. H. is grateful for the financial support from the National Natural Science Foundation of China (grant no. 21379105). It is also supported by the China Postdoctoral Science Foundation (grant no. 2013M541655) and Jiangsu Planned Projects for Postdoctoral Research Funds (grant no. 1301039B).

Notes and references

1 F. Auzel, *Chem. Rev.*, 2003, **104**, 139–174.
2 S. Gai, C. Li, P. Yang and J. Lin, *Chem. Rev.*, 2014, **114**, 2343–2389.
3 F. Auzel, *J. Lumin.*, 1990, **45**, 341–345.
4 M. Haase and H. Schäfer, *Angew. Chem., Int. Ed.*, 2011, **50**, 5808–5829.
5 P. P. Feofilov and V. V. Ovsyankin, *Appl. Opt.*, 1967, **6**, 1828–1833.
6 G. Wang, Q. Peng and Y. Li, *Acc. Chem. Res.*, 2011, **44**, 322–332.
7 L. Cheng, C. Wang and Z. Liu, *Nanoscale*, 2013, **5**, 23–37.
8 J. Zhou, Z. Liu and F. Li, *Chem. Soc. Rev.*, 2012, **41**, 1323–1349.
9 F. Chen, W. Bu, S. Zhang, J. Liu, W. Fan, L. Zhou, W. Peng and J. Shi, *Adv. Funct. Mater.*, 2013, **23**, 298–307.
10 L.-L. Li, P. Wu, K. Hwang and Y. Lu, *J. Am. Chem. Soc.*, 2013, **135**, 2411–2414.
11 S. Zeng, J. Xiao, Q. Yang and J. Hao, *J. Mater. Chem.*, 2012, **22**, 9870–9874.
12 J. Wu, Q. Tian, H. Hu, Q. Xia, Y. Zou, F. Li, T. Yi and C. Huang, *Chem. Commun.*, 2009, 4100–4102.
13 J. Zhou, X. Zhu, M. Chen, Y. Sun and F. Li, *Biomaterials*, 2012, **33**, 6201–6210.
14 X.-F. Qiao, J.-C. Zhou, J.-W. Xiao, Y.-F. Wang, L.-D. Sun and C.-H. Yan, *Nanoscale*, 2012, **4**, 4611–4623.
15 F. Wang, R. Deng, J. Wang, Q. Wang, Y. Han, H. Zhu, X. Chen and X. Liu, *Nat. Mater.*, 2011, **10**, 968–973.
16 Y. Yang, F. Liu, X. Liu and B. Xing, *Nanoscale*, 2013, **5**, 231–238.
17 L. Wang, J. Liu, Y. Dai, Q. Yang, Y. Zhang, P. Yang, Z. Cheng, H. Lian, C. Li, Z. Hou, P. a. Ma and J. Lin, *Langmuir*, 2014, **30**, 13042–13051.
18 D. Yang, Y. Dai, J. Liu, Y. Zhou, Y. Chen, C. Li, P. a. Ma and J. Lin, *Biomaterials*, 2014, **35**, 2011–2023.
19 F. Wang and X. Liu, *Chem. Soc. Rev.*, 2009, **38**, 976–989.
20 Z.-G. Yan and C.-H. Yan, *J. Mater. Chem.*, 2008, **18**, 5046–5059.
21 N. Bogdan, F. Vetrone, G. A. Ozin and J. A. Capobianco, *Nano Lett.*, 2011, **11**, 835–840.
22 F. Wang, X. Xue and X. Liu, *Angew. Chem., Int. Ed.*, 2008, **47**, 906–909.
23 K. Li, M. Shang, D. Geng, H. Lian, Y. Zhang, J. Fan and J. Lin, *Inorg. Chem.*, 2014, **53**, 6743–6751.
24 C. Li and J. Lin, *J. Mater. Chem.*, 2010, **20**, 6831–6847.
25 S. Heer, K. Kömpe, H. U. Güdel and M. Haase, *Adv. Mater.*, 2004, **16**, 2102–2105.
26 S. Sivakumar, F. C. J. M. van Veggel and M. Raudsepp, *J. Am. Chem. Soc.*, 2005, **127**, 12464–12465.
27 L. Wang, M. Lan, Z. Liu, G. Qin, C. Wu, X. Wang, W. Qin, W. Huang and L. Huang, *J. Mater. Chem. C*, 2013, **1**, 2485–2490.
28 K. Deng, T. Gong, L. Hu, X. Wei, Y. Chen and M. Yin, *Opt. Express*, 2011, **19**, 1749–1754.
29 F. Liu, Q. Zhao, H. You and Z. Wang, *Nanoscale*, 2013, **5**, 1047–1053.
30 S. Schietinger, T. Aichele, H.-Q. Wang, T. Nann and O. Benson, *Nano Lett.*, 2009, **10**, 134–138.
31 J.-C. Boyer, J. Gagnon, L. A. Cuccia and J. A. Capobianco, *Chem. Mater.*, 2007, **19**, 3358–3360.
32 Q. Xiao, Y. Ji, Z. Xiao, Y. Zhang, H. Lin and Q. Wang, *Chem. Commun.*, 2013, **49**, 1527–1529.
33 C. Li, Z. Hou, C. Zhang, P. Yang, G. Li, Z. Xu, Y. Fan and J. Lin, *Chem. Mater.*, 2009, **21**, 4598–4607.
34 H. H. Gorris and O. S. Wolfbeis, *Angew. Chem., Int. Ed.*, 2013, **52**, 3584–3600.
35 B. Zhou, Y. Idobata, A. Kobayashi, H. Cui, R. Kato, R. Takagi, K. Miyagawa, K. Kanoda and H. Kobayashi, *J. Am. Chem. Soc.*, 2012, **134**, 12724–12731.
36 G. Tian, Z. Gu, L. Zhou, W. Yin, X. Liu, L. Yan, S. Jin, W. Ren, G. Xing, S. Li and Y. Zhao, *Adv. Mater.*, 2012, **24**, 1226–1231.
37 S. Gai, C. Li, P. Yang and J. Lin, *Chem. Rev.*, 2013, **114**, 2343–2389.
38 H. Na, J. Jeong, H. Chang, H. Kim, K. Woo, K. Lim, K. A. Mkhoyan and H. Jang, *Nanoscale*, 2014, **6**, 7461–7468.
39 Y. Liu, D. Tu, H. Zhu and X. Chen, *Chem. Soc. Rev.*, 2013, **42**, 6924–6958.
40 F. Wang and X. Liu, *Acc. Chem. Res.*, 2014, **47**, 1378–1385.
41 H. Na, K. Woo, K. Lim and H. S. Jang, *Nanoscale*, 2013, **5**, 4242–4251.
42 Y. Ai, D. Tu, W. Zheng, Y. Liu, J. Kong, P. Hu, Z. Chen, M. Huang and X. Chen, *Nanoscale*, 2013, **5**, 6430–6438.

43 H. Fu, G. Yang, S. Gai, N. Niu, F. He, J. Xu and P. Yang, *Dalton Trans.*, 2013, **42**, 7863–7870.
44 X. Teng, Y. Zhu, W. Wei, S. Wang, J. Huang, R. Naccache, W. Hu, A. I. Y. Tok, Y. Han, Q. Zhang, Q. Fan, W. Huang, J. A. Capobianco and L. Huang, *J. Am. Chem. Soc.*, 2012, **134**, 8340–8343.
45 X. Liang, X. Wang, J. Zhuang, Q. Peng and Y. Li, *Adv. Funct. Mater.*, 2007, **17**, 2757–2765.
46 N. C. Seeman, *Nature*, 2003, **421**, 427–431.
47 H. Qiu, G. Chen, L. Sun, S. Hao, G. Han and C. Yang, *J. Mater. Chem.*, 2011, **21**, 17202–17208.
48 Y. Ding, X. Teng, H. Zhu, L. Wang, W. Pei, J.-J. Zhu, L. Huang and W. Huang, *Nanoscale*, 2013, **5**, 11928–11932.
49 L. Wang, H. Chen, D. Zhang, D. Zhao and W. Qin, *Mater. Lett.*, 2011, **65**, 504–506.
50 L. Wang, X. Xue, F. Shi, D. Zhao, D. Zhang, K. Zheng, G. Wang, C. He, R. Kim and W. Qin, *Opt. Lett.*, 2009, **34**, 2781–2783.
51 M. Pang, J. Feng, S. Song, Z. Wang and H. Zhang, *CrystEngComm*, 2013, **15**, 6901–6904.
52 S. Hao, L. Sun, G. Chen, H. Qiu, C. Xu, T. N. Soitah, Y. Sun and C. Yang, *J. Alloys Compd.*, 2012, **522**, 74–77.